



Research article

The synergistic effects of green-blue-gray infrastructure for flood risk management in plain river network areas



Haoxun Zhang ^{a,b}, Qichen Hong ^a, Yutong Jiang ^a , Yuting Xie ^{a,c,*}

^a Institute of Landscape Architecture, College of Agriculture and Biotechnology, Zhejiang University, Hangzhou, 310058, China

^b Center for Balance Architecture, Zhejiang University, Hangzhou, 310058, China

^c Zhejiang University Architectural Design and Research Institute Co., Ltd, Hangzhou, 310058, China

ARTICLE INFO

Handling Editor: Jason Michael Evans

Keywords:

Climate adaptation
Synergistic effect
Green-blue-gray infrastructure
Flood risk management
Resilience planning
Depoldering

ABSTRACT

Climate change and urbanization have heightened flood risks by intensifying rainfall and expanding impervious surfaces, underscoring the need to integrate green, blue, and gray infrastructure (GBGI) as adaptive strategies. However, most studies examine GBGI at building or block scales, prioritizing expanding low-resilience gray infrastructure. They also lack standardized methodologies for quantifying synergistic effects, with scant mechanistic insight and rarely consider contextual drivers like rainfall intensity or spatial heterogeneity. We address these gaps at watershed scale in a plain river network region, simulating seven GBGI scenarios—green, blue, gray (depoldering), and four combinations—with an SCS-MIKE11 hydrological-hydrodynamic model for 20-, 50-, and 100-year rainfall events. Synergistic effects were assessed by the difference between combined and summed individual strategies performance via reduction rates of maximum water level (MWL), peak discharge (PD), and flooding rate (FR). Results show that (1) gray strategy through large-scale depoldering demonstrates significant flood risk management performance across all scenarios (MWL 2.34–2.46 %, PD 1.16–1.39 %, FR 4.70–16.32 %), highlighting the value of restoring hydrological connectivity; (2) blue-gray and green-blue-gray strategies generate robust positive synergies (0.98–4.92 %) concentrated upstream, whereas green-blue and green-gray mixes deliver limited or negative effects (down to –1.55 %), due to infrastructural interactions in runoff generation, storage, and drainage within polders; (3) rainfall intensity differentially influences synergistic effects, with MWLs showing minimal sensitivity (variation $\leq 0.24 \%$), PDs increasing from 0.10 % to 1.20 % with rising intensity, and FRs reaching peak synergy at 50-year return period (5.71 %). These findings advance watershed-scale GBGI synergistic effect theory and provide location- and event-specific guidance for climate-adaptive infrastructure planning.

1. Introduction

In the context of global climate change, the frequency and intensity of extreme precipitation events are on the rise, leading to frequent urban flooding disasters (Hosseinzadehtalaei et al., 2020). Concurrently, rapid urbanization worldwide is driving significant changes in land use of underlying surfaces. The substantial increase in impervious surfaces in urban areas has augmented water yield and peak flow, thereby exacerbating flood risks (Li et al., 2013; Suriya and Mudgal, 2012).

To address flood risk as a core climate adaptation challenge, traditional flood risk management followed an "add-more-gray" logic: the growing gray infrastructure (dikes, sluices, and pipes) guaranteed

hydraulic control but at high financial and ecological cost (Tavakol-Davani et al., 2016). In the Netherlands, public opposition to large-scale flood protection infrastructure programme during the 1970s sparked an "ecological conceptualization" of flood management (Bijker, 2002; Disco, 2002). Policy frameworks such as *Dealing with Water* (Min VenW, 1985) formalized this shift, integrating ecological insights and spatial planning into flood decisions (Saeijs, 2008; Van Hemert, 2008; Wiering and Arts, 2006). A hallmark of the new approach is depoldering or managed realignment—breaching or relocating dikes to reopen floodplains and restore natural dynamics (van Staveren et al., 2014; Bax et al., 2023). Pioneered by the Dutch *Room for the River* program—which recast dikes as regulators of controlled inundation, combining flood

* Corresponding author, 866 Yuhangtang Road, Institute of Landscape Architecture, College of Agriculture and Biotechnology, Zhejiang University, Hangzhou, 310058, China.

E-mail address: xieyuting@zju.edu.cn (Y. Xie).

safety with habitat gains (Rijke et al., 2012; Schut et al., 2010)—depoldering has since proved its worth elsewhere in Europe: the 465 ha Hedwige-Prosper realignment, for example, both lowered flood peaks and generated extensive tidal wetlands, confirming the strategy's dual benefits for flood protection and ecological restoration (European Environment Agency, 2023). A parallel evolution is under way in China's Yangtze River Delta. Centuries of dike-and-pump construction have produced a dense polder system that internally lowers flood risk yet reduces basin-scale storage and regulation capacity (Y. Gao et al., 2023). The legally binding *Territorial Master Plan for the Ecological Green Integration Demonstration Zone* (2021–2035) now bans new hard defenses and mandates depoldering to reconnect flows, enlarge water surfaces, and add ecological land, thereby strengthening flood resilience and biodiversity. Building on these European and Chinese initiatives, global climate-adaptation agendas now prioritize nature-based approaches—sponge cities, water-sensitive urban design, resilient landscapes—that weave green and blue infrastructure into a streamlined gray framework (Alves et al., 2018; Casal-Campos et al., 2018; Ncube and Arthur, 2021; Rosa et al., 2020). These measures—including urban green spaces, forests, rivers, lakes and retention facilities (Ghofrani et al., 2017)—not only attenuate runoff but also deliver long-term ecological and environmental co-benefits, being increasingly favored for supporting both resilience and economic sustainability (Dong et al., 2017; Lu et al., 2023).

Building on this paradigm, recent studies increasingly highlight the added value of fully integrating green, blue, and gray infrastructure (GBGI) for flood risk management as a comprehensive climate adaptation approach. Research consistently shows that combined GBGI strategies outperform individual infrastructure solutions (Al-Humaiqani and Al-Ghamdi, 2023; Bakhshipour et al., 2019; Yin et al., 2023). Performance evaluations conducted at building and block scales for various combinations of green (e.g., green spaces, green roofs, bioswales), blue (e.g., retention basins), and gray (e.g., permeable pavements, storm-water networks) infrastructure have revealed that green-blue-gray strategies consistently achieve the most significant runoff reduction across different rainfall intensities (Martínez et al., 2021; Versini et al., 2018; Yin et al., 2023). Further studies at city and watershed scales have confirmed that combined GBGI strategies, such as the implementation of sponge city measures, depoldering, and restoration of lake areas, outperform individual infrastructure approaches in enhancing flood storage capacity, reducing peak discharge, shortening flood duration, and minimizing inundation area (Lan, 2023; Xu et al., 2019). Although these findings are promising, there is still limited research that provides definitive evidence of synergistic effects from such combinations.

Synergistic effects refer to a phenomenon in which the combined performance of multiple strategies or measures exceeds the sum of their individual performances, resulting in a greater overall effect (Geary, 2013; Rehak et al., 2016). Yet GBGI studies still apply this concept unevenly. Some papers merely assert synergy without quantification: Zeng et al. (2019) demonstrated that combining green infrastructures like rain gardens and sunken green spaces with gray infrastructures such as drainage pipes can produce synergistic effects. However, their study was unable to fully quantify these effects due to the absence of a complete experimental control group. Similarly, Martínez et al. (2021) and Pamungkas and Purwitaningsih (2019) found Green-gray combinations effective for flood damage and runoff reduction, though they did not measure the difference between combined and individual performances. Others infer synergy but use inconsistent component sets: J. Chen et al. (2024) expanded the analysis by incorporating blue infrastructure and identified the Green-gray-blue strategy as the most effective for flood risk reduction, but did not standardize the extents of each component before comparison. Only a few studies apply a rigorous, additive benchmark: J. Wang et al. (2022) held intervention extents constant, then directly contrasted combined strategy performance with the summed performance of its individual parts—thereby providing a reproducible measure of synergy. Even among these rigorous studies,

conclusions diverge and the mechanisms behind any synergy remain obscure.

Three further gaps limit current understanding. First, scale: most interaction tests stay at building or block level (J. Chen et al., 2024; Martínez et al., 2021; Wang et al., 2022; Zeng et al., 2019), with only scattered watershed-scale work and inconsistent results (Pamungkas and Purwitaningsih, 2019; Wang et al., 2022; Zhang et al., 2023). Second, the nature of the gray component: research almost always studies adding infrastructure, whereas large-scale depoldering—removing dikes to reopen floodplains—has not been systematically analyzed. Third, context sensitivity: little is known about how synergy varies with external drivers. The impact of rainfall intensity on synergistic effect has scarcely been tested, and the spatial heterogeneity of synergistic effects remains largely unexplored.

To address these research gaps, this study examines the synergistic effects of GBGI strategies for flood risk management and their sensitivity to rainfall intensity in a flood-prone plain in the Yangtze River Delta, China. We designed seven scenarios encompassing individual and combined GBGI strategies under 20-year, 50-year, and 100-year return periods. A hydrological-hydrodynamic coupling model simulated flood processes and evaluated the reduction rates of maximum water level (MWL), peak discharge (PD), and flooding rate (FR). By comparing the performances of combined GBGI strategies with individual ones across different rainfall intensities, this study verifies synergistic effects at the watershed scale and maps their spatial heterogeneity along the river network. The resulting insights inform location- and event-specific GBGI combinations, providing scientific guidance for land-use planning and watershed-level flood-resilience enhancement.

2. Materials

2.1. Study area

This study focuses on the Yangtze River Delta Ecological Green Integration Demonstration Zone. This zone includes Qingpu District in Shanghai, Wujiang District in Suzhou, Jiangsu Province, and Jiashan County in Jiaxing, Zhejiang Province, covering a total area of approximately 2413 km² (Fig. 1a). With a typical plain river network, the area is particularly vulnerable to flooding due to its low-lying terrain, with an average altitude of no more than 5 m (Wu et al., 2020). The flooding issue is further exacerbated by the reduction of permeable surfaces, as this region is among the most urbanized in China (Fig. 1b).

To mitigate flood risks, polders, which are low-lying areas reclaimed from water bodies, have been continuously consolidated and maintained using multi-level dikes, sluices, and pumps (B. Gao et al., 2023). Therefore, the study area is divided into 332 polder catchments and 26 non-polder catchments (Fig. 1c).

The systematic establishment of polders has led to the formation of a comprehensive GBGI system within study area. In this plain river network region with widespread polder fields, green infrastructure consists of ecological land (primarily woodland) that enhances infiltration and reduces runoff. Blue infrastructure comprises water bodies (lakes, ditches, and ponds) that provide water storage and regulation. Gray infrastructure includes hydraulic infrastructure (dikes, sluices and pumps) that regulate water movement by closing sluices during high external water levels to prevent backflow, and by either opening sluices for gravity drainage or operating pumps for forced drainage when external water levels are low. The extent and connectivity of the green and blue infrastructure play a critical role in enhancing flood retention capacity (Wang et al., 2016). While the gray infrastructure provides essential protection within polder catchments, it also accelerates water level rise in the external river network during flood seasons, thereby exacerbating regional flooding conditions (Cheng and Wu, 2019).

Based on understanding of the GBGI system's functional mechanisms in the study area, we developed green, blue and gray strategies to design various scenarios, examining the synergistic effects of GBGI strategies on

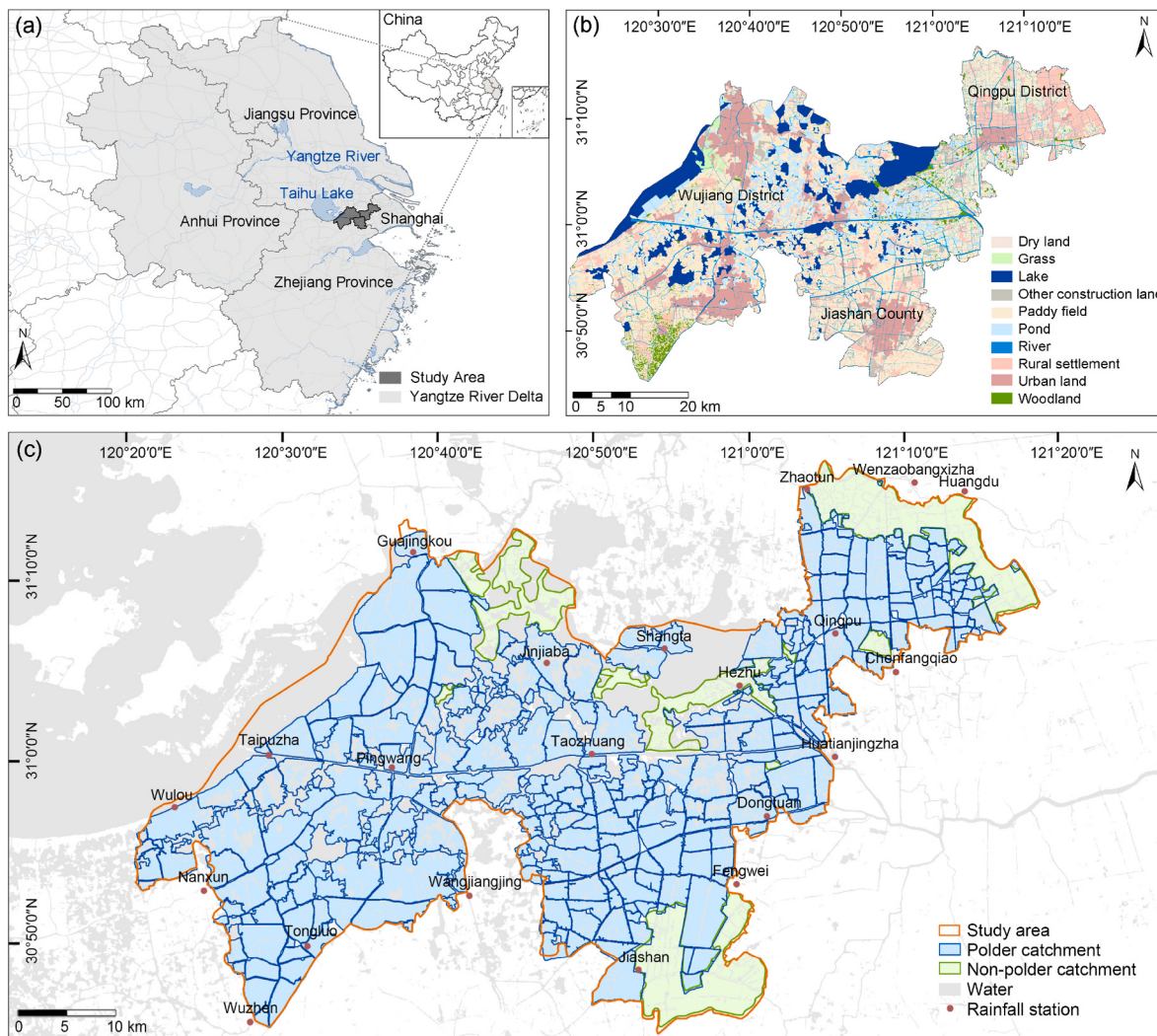


Fig. 1. Study area of the Yangtze River Delta Ecological Green Integration Demonstration Zone. (a) Geographic location; (b) Land use type; (c) Division of polder and non-polder catchments.

flood risk management.

2.2. Data preparation

The main data used in this study includes land use and land cover (LULC), digital elevation model (DEM), hydrological and hydrodynamic data, water system and its cross-section data, and data on water conservancy project. Detailed data sources are provided in Appendix A, Table A.1. We used 30m resolution land use data from the Chinese Academy of Sciences, which was corrected for woodland areas using the European Space Agency's global 10m resolution land cover data. This integration of open-source data significantly improved the accuracy of LULC, contributing to more precise runoff calculations. Hydrological and hydrodynamic data includes daily rainfall data from 21 rainfall stations in the study area, as well as daily average water level, tide level, and flow data from 20 hydrological stations (Appendix A; Table A.2-A.7). Additionally, due to incomplete river cross-section information obtained from local chronicles, we supplemented and corrected this data using DEM data. We also acquired hydraulic engineering maps of the study area, which provide the distribution of dikes, sluices and pump stations in all polder catchments in the study area.

3. Methods

This study employs a framework that enables a systematic analysis of GBGI strategies' synergistic effects across different spatial scales and rainfall intensities, providing insights into their impacts and mechanisms on flood risk mitigation. The overall framework includes three components (Fig. 2): (1) scenarios design, which included the development of rainfall scenarios based on three return periods (20-year, 50-year, and 100-year) and the creation of seven GBGI strategy scenarios in both individual and combined forms; (2) hydrological-hydrodynamic modeling using a coupled SCS-MIKE11 model to simulate flood processes under various scenarios; (3) synergistic effect assessment, which involves calculating performance indicators to determine MWLs, PDs, and FRs. This is followed by evaluating the performance and synergistic effects of strategies, examining the underlying mechanisms, and assessing the impact of rainfall intensity on synergistic effect.

3.1. Scenario design

3.1.1. Rainfall scenario design

Based on the design rainfall analysis of the "Design Rainfall Revision of Taihu Basin" (Hu et al., 2016) and the hydrological sub-regional precipitation data of the study area, both the typical 15-day cumulative rainfall depths and their corresponding daily distribution patterns

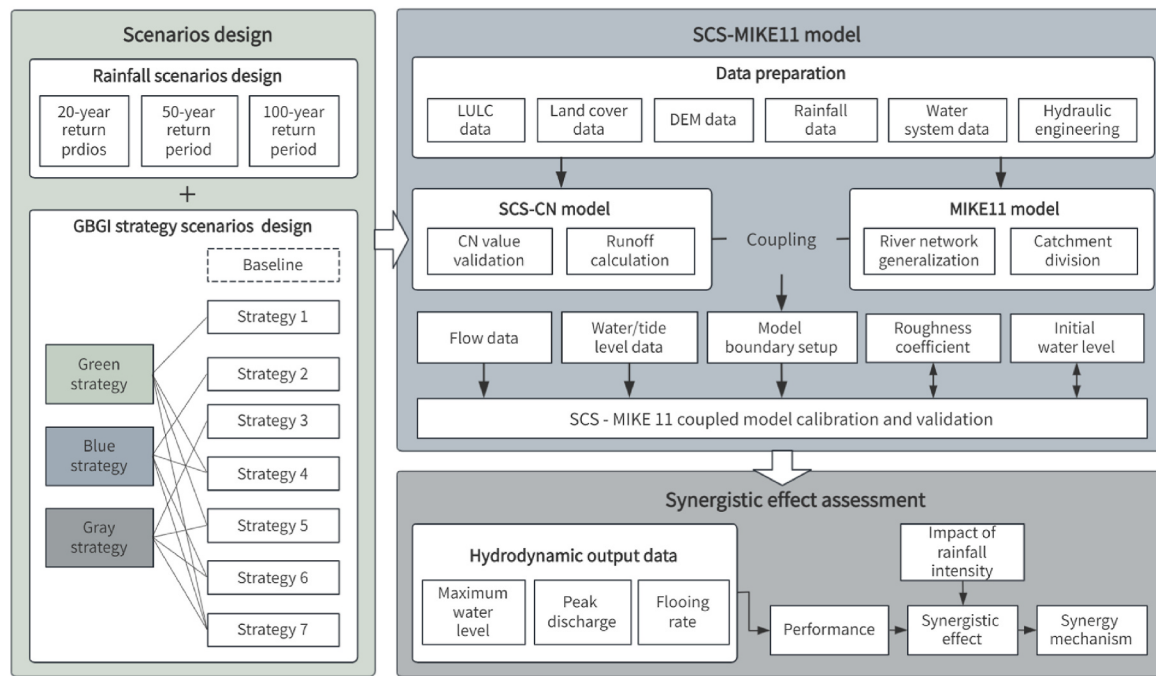


Fig. 2. Overall framework of the study.

were determined. Through frequency-consistent amplification methodology, the daily rainfall distribution sequences for 20-year, 50-year, and 100-year return periods were derived from the maximum 15-day design rainfall patterns. These return periods align with the official flood protection standards established in the Territorial Master Plan for the Yangtze River Delta Ecological Green Integration Demonstration Zone (2021–2035), where urban areas meet 100-year flood protection standards and 20-year return period drainage standards, other areas require 50-year flood protection standards, and rural areas require drainage standards for 20-year return period rainfall events. Details of the daily rainfall distribution patterns are provided in Fig. 3.

3.1.2. GBGI strategy scenario design

To enhance climate adaptation, the study area's territorial planning proposes optimizing hydrological functions, including increasing water storage capacity, reducing water level, and regulating flow, to strengthen flood resilience. These objectives are supported by ecological restoration, expanding water surfaces, and limiting polder consolidation

while promoting depoldering through adjustments in land use and polder management. Building on the GBGI system described in Section 2.1, our proposed GBGI strategy scenarios align with the planning goals: For the green strategy, we selected paddy field-woodland conversion as woodland constitutes the predominant ecological land type in the study area (Fig. 1b) and has lower CN values than paddy fields (Table 2), indicating superior infiltration capacity. The blue strategy expands water surface areas for enhanced storage. Our gray strategy uniquely focuses on depoldering (removing dikes, sluices, and pumps) to restore hydrological connectivity between polders and external waters, enhancing the overall watershed regulation and retention capacity, aligning with the contemporary trend of gray infrastructure intervention that encompass both construction and strategic removal for climate adaptation.

Based on the 2020 land use data and the 2019 hydraulic engineering layout of the study area, this study established a baseline scenario. Our baseline land use analysis shows that paddy field constitute 46.2 % of the total area, followed by rural settlement (15.8 %), water body (13.7

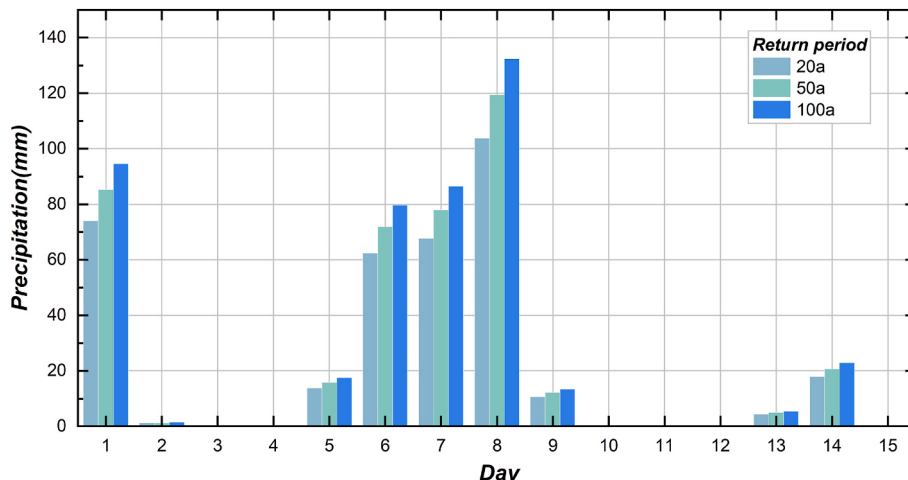


Fig. 3. Daily distribution of design rainfall in the study area.

Table 1
GBGI strategy scenarios design.

Scenarios	Strategy type	Description
Baseline	None	2020 land use data and the 2019 hydraulic infrastructure layout
Strategy 1	Green	Convert 10 % paddy field to woodland
Strategy 2	Blue	Convert 10 % paddy field to ditches or ponds
Strategy 3	Gray	Depoldering polder catchments
Strategy 4	Green-blue	Convert 10 % paddy field to woodland, and 10 % paddy field to ditches or ponds
Strategy 5	Green-gray	Convert 10 % paddy field to woodland and depolder the corresponding polder catchments
Strategy 6	Blue-gray	Convert 10 % of the paddy fields into ditches or ponds and depolder the corresponding polder catchments
Strategy 7	Green-blue-gray	Convert 10 % paddy field to woodland, 10 % paddy field to ditches or ponds and depolder the corresponding polder catchments

Table 2
Calibrated CN values for the study area.

Land use type	CN1	CN2	CN3
Paddy field	91	97	99
Dry land	75	88	95
Woodland	72	86	94
Grass	57	75	88
Water	100	100	100
Other construction land	66	82	92
Rural land	66	82	92
Urban land	85	94	98

%), woodland (13.1 %), urban land (8.5 %), other construction land (2.1 %), grass (0.3 %), and dry land (0.3 %). Based on this baseline, we developed seven strategy scenarios employing green, blue, and gray strategies individually (Strategies 1–3) or in combination (Strategies 4–7) (Table 1). Each strategy scenario was compared with the baseline scenario to evaluate its flood risk management performance. For the combined strategies in Strategies 4–7, their performances were compared with the sum of the corresponding individual strategies to calculate synergistic effects. It is important to note that for combined strategies (Strategies 4–7), the intervention extents are equivalent to the sum of their corresponding individual strategies, ensuring fair and methodologically reasonable comparisons.

These strategies were implemented only in polder catchments, as these areas serve as the basic units for flood management and the only catchments where the gray strategy can be applied. To ensure accurate assessment of synergistic effects, it was crucial to select polder catchments capable of implementing all GBGI strategies. Additionally, these strategies needed to be effectively applied to a substantial proportion of the polder areas to ensure significant impacts. Therefore, we selected polder catchments with more than 20 % paddy field, where individual green (converting 10 % to woodland), blue (converting 10 % to ditches or ponds), and gray (depoldering) strategies, as well as their combination, could be implemented. A total of 272 polder catchments were selected for conversion—81.9 % of all polders—restoring natural hydrological connectivity across 168 km² water, and converting 1033 km² land from controlled to naturally drainage, totaling 1201 km² (Fig. 4a).

3.2. SCS-MIKE11 model

In our study area, the hydrological processes involve complex interactions between external river network and 358 polders/non-polder catchments, requiring a model that can simulate both internal runoff generation and external flow routing. We developed a coupled SCS-

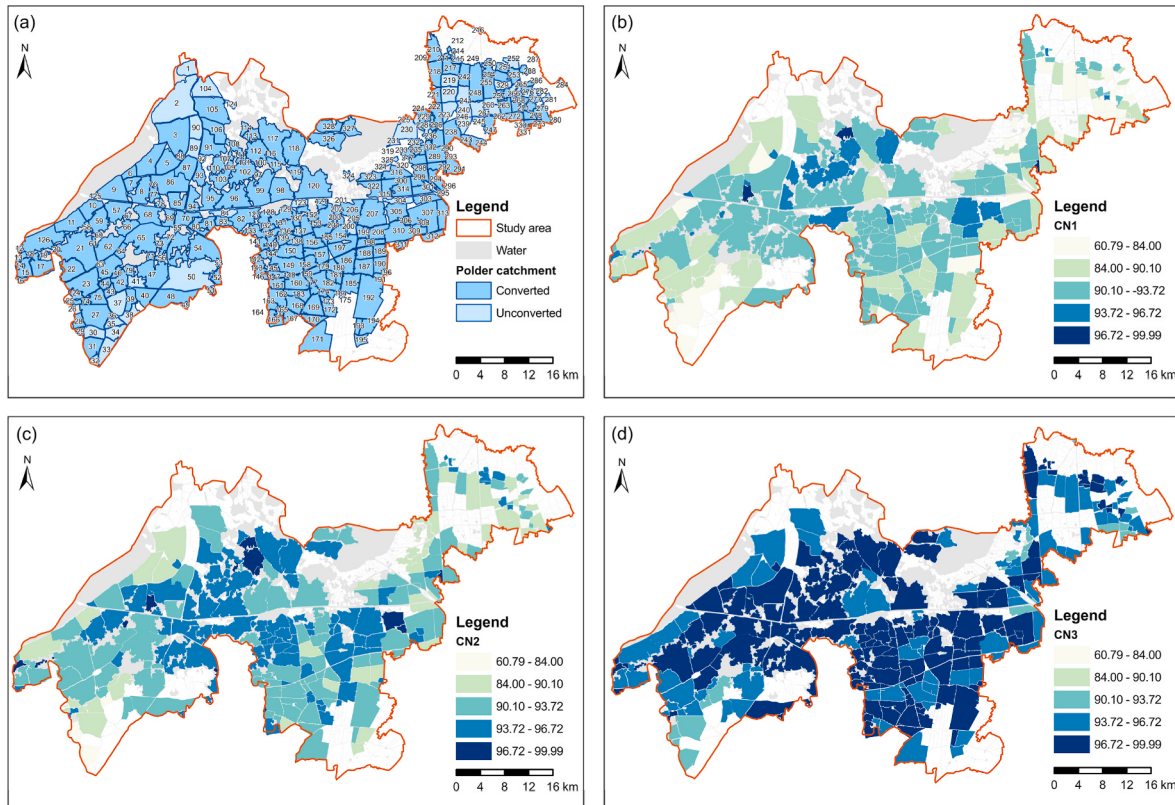


Fig. 4. Distribution of converted polder catchments and their CN values. (a) Distribution of the 272 converted polder catchments; (b) CN1 values (dry conditions); (c) CN2 values (moderately wet conditions); (d) CN3 values (wet conditions).

MIKE11 hydrological-hydrodynamic model to simulate the flood processes of the study area under different scenarios.

The SCS model fits plain river network areas where measured flow data are scarce (Gan et al., 2010). It can reflect the land use situation in the study area and the corresponding runoff under different rainfall conditions (Beilicci and Beilicci, 2024). MIKE11, a widely used one-dimensional hydrodynamic model, is suitable for plain river network regions to simulate flood processes and generate data on water levels, discharges, and other relevant hydrodynamic information (Zhong et al., 2017). Therefore, the SCS-MIKE11 coupled model effectively captures the hydraulic connections between polder areas and external rivers as well as simulates flood processes (Drobot and Draghia, 2014; Han et al., 2014; Luo et al., 2018). This coupled model effectively represents green and blue infrastructure strategies through land use changes and simulates flood processes controlled by gray infrastructure through setting specific model boundaries and runoff routing methods (Gao et al., 2023).

3.2.1. SCS model and CN value calibration

The SCS model, developed by the Soil Conservation Service of the United States Department of Agriculture (USDA), is a watershed hydrology model that has been extensively used and validated by numerous scholars over the years (Soulis, 2021). It considers the impact of soil type, land use, and antecedent soil moisture on rainfall runoff. The SCS model runoff calculation formula is:

$$Q = \begin{cases} \frac{(P - 0.05S)^2}{P + 0.95S}, & P \geq 0.05S \\ 0, & P < 0.05S \end{cases} \quad (1)$$

Where S is the maximum potential retention of the watershed, in mm; Q is the runoff depth, in mm; P is the rainfall amount, in mm.

In the SCS-CN model, the CN value is a comprehensive parameter that characterizes land use types and soil hydraulic properties. The relationship between the maximum potential retention S and the runoff curve number CN is:

$$S = \frac{25400}{CN} - 254 \quad (2)$$

The Soil Conservation Service (SCS) developed a runoff curve number table based on a large amount of measured data. The predominant soil type in the study area is paddy loam, classified as type C (low infiltration). As the soil conditions in China differ from those in the United States, this study referred to CN value calibration research in Taihu Basin (Zhang et al., 2014) and Yangtze River Delta (Liu, 2007) to create a set of runoff curve numbers suitable for the study area (Table 2).

Based on the antecedent rainfall conditions, the soil moisture conditions were divided into three categories: AMC I (dry), AMC II (moderately wet), and AMC III (wet). The CN values were adjusted using the formula:

$$CN_I = 4.2CN_{II} / (10 - 0.058CN_{II}) \quad (3a)$$

$$CN_{III} = 23CN_{II} / (10 + 0.13CN_{II}) \quad (3b)$$

Finally, the weighted CN values for each catchment area was calculated according to the proportion of each land use type in the total area (Fig. 4b-d).

3.2.2. MIKE11 model construction

The numerous rivers and lakes of the study area were digitized in ArcGIS and generalized into river networks model and storage nodes in MIKE11. The river cross-sections were extracted and generalized into trapezoidal shapes based on water system data and DEM data of the study area. To meet the computational requirements of MIKE's hydrodynamic module, interpolated cross-sections were generated at 100-m intervals between actual surveyed cross-sections throughout the river

network. The river network of model extended to flow level stations as upstream boundaries, and water level or tide level stations as downstream boundaries. Fig. 5 shows the constructed MIKE11 model, including 165 generalized rivers, 11 storage nodes, 13,238 river cross-sections, 3 upstream boundaries, and 7 downstream boundaries.

3.2.3. SCS-MIKE11 coupled model setup

Based on the actual distribution of polders and the dispatch rules of pumping stations in the study area, two types of catchments were delineated: polder and non-polder. The SCS model calculated the daily runoff volume for each catchment. Following the "Taihu Basin Model" (Cheng et al., 2006), distinct routing processes were applied to each catchment type. For polder catchments, the runoff routing process was considered negligible owing to the relatively small spatial extent and limited routing distances. Consequently, the calculated runoff volume was directly added to each polder's water surface. When the water depth exceeded the maximum storage depth (0.40 m), the pumping stations would be activated to discharge the excess runoff volume into the external river network (Cheng and Wu, 2019). For non-polder catchments, the 4-4-2 runoff routing process, as characterized in the "Taihu Basin Model", was adopted, i.e., 40 % of the runoff on the day of generation flowed into the river network, with 40 % and 20 % flowing in on the second and third days, respectively.

Moreover, different forms of internal boundaries were added to the MIKE11 model to couple the polder and non-polder catchments with the river network (Fig. 6) (Han et al., 2014). For polder catchments, point source boundaries were set at pumping station locations to simulate flood discharge from the polder into the river network. For non-polder catchments, distributed source boundaries were set around the river network to simulate the dispersed runoff into the river network. In our study, the gray strategy converts 272 polder catchments to non-polder catchments, therefore, their water body areas are integrated into the external river network and computed within MIKE11, while the non-water areas transition from polder to non-polder runoff routing processes after runoff generation.

3.2.4. Model calibration and validation

To ensure the reliability of the SCS-MIKE11 model, calibration and validation were conducted. The difference of maximum water levels and RMSE were selected as primary validation metrics, directly corresponding to the flood risk mapping handbook requirements which stipulate that the difference between calculated and observed maximum water levels should generally not exceed 20 cm, while the water level variation trends between calculated and observed values should be reasonably similar (China Institute of Water Resources and Hydropower Research, 2010).

The initial roughness coefficient (Manning's n) was set to 0.03, which has been commonly used in Taihu Basin (Zhao et al., 2022). The initial water level was set to 2.80 m according to the average value of the local water level stations in June. The flood period from June 1 to 13, 2020, was selected for calibration, as it corresponds to a typical rainfall event, and the measured water levels during this time were close to the area's annual average, thus aligning well with most scenarios. The calculated water levels at 3 water level stations (Pingwang, Zhaotun, Shangta) were compared with the measured daily average water levels, based on which model parameters were further adjusted. After parameter calibration, the flood induced by Typhoon "Meihua" from September 12 to 24, 2020, were selected for validation. Finally, the riverbed roughness coefficient ranged from 0.03 to 0.06, and the initial water level was adjusted to 3.00 m. The water level deviation met the validation requirements (Table 3), indicating that the model could effectively simulate the rainfall and flood processes in the study area.

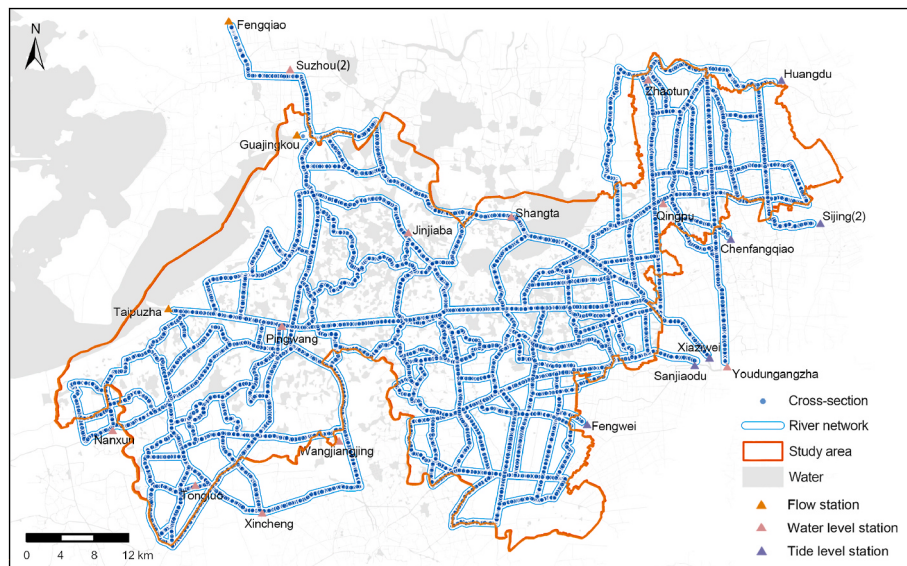


Fig. 5. Constructed MIKE11 model with river networks, cross-section distribution, and hydrological station locations.

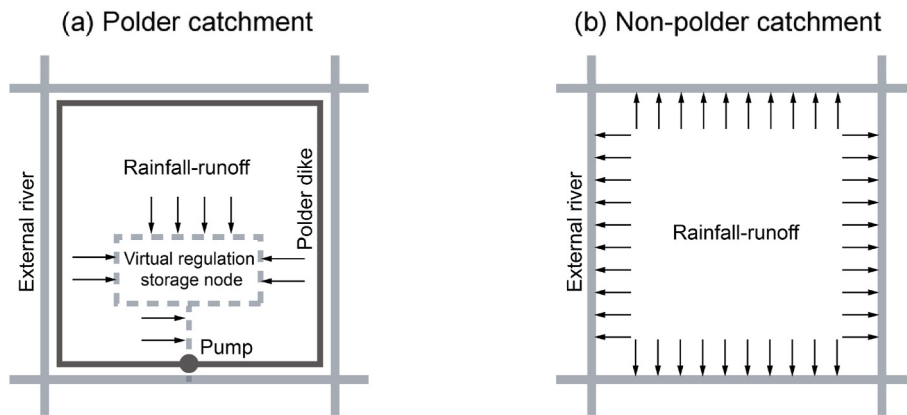


Fig. 6. Runoff routing methods for polder and non-polder catchments, adapted from Han et al. (2014).

3.3. Performance indicators and synergistic effect calculation

3.3.1. Performance indicators calculation

In this study, three indicators were used to evaluate the performances of different GBGI strategies for flood risk management: reduction rates of maximum water level (MWL), peak discharge (PD), and flooding rate (FR). These indicators were calculated using the hydrological and hydrodynamic data obtained from the river network within the study area, which includes 13,238 cross-sectional nodes (see Fig. 5).

(1) Reduction rate of maximum water level (MWL)

MWL is calculated as the average of maximum water level reduction rates across all cross-sections by comparing the baseline scenario with the strategy scenarios. The formula used is:

$$\left\{ \begin{array}{l} R_{MWL,i}(X) = \left(\frac{MWL_{B,i} - MWL_i(X)}{MWL_{B,i}} \right) \times 100\% \\ R_{MWL}(X) = \frac{\sum R_{MWL,i}(X)}{N} \end{array} \right. \quad (4)$$

Where $R_{MWL,i}(X)$ is the MWL for cross-section i in strategy scenario X (%); $MWL_{B,i}$ is the maximum water level in baseline scenario for cross section i (m); $MWL_i(X)$ is the maximum water level in strategy scenario

X for cross-section i (m); $R_{MWL}(X)$ is the average MWL across all cross-sections for strategy scenario X (%); N is the total number of cross-sections.

(2) Reduction rate of peak discharge (PD)

PD is calculated as the average of peak discharge reduction rates across all cross-sections. The formula used is:

$$\left\{ \begin{array}{l} R_{PD,i}(X) = \left(\frac{PD_{B,i} - PD_i(X)}{PD_{B,i}} \right) \times 100\% \\ R_{PD}(X) = \frac{\sum R_{PD,i}(X)}{N} \end{array} \right. \quad (5)$$

Where $R_{PD,i}(X)$ is the PD for cross-section i in strategy scenario X (%); $PD_{B,i}$ is the peak discharge in baseline scenario for cross-section i (m^3/s); $PD_i(X)$ is the peak discharge in strategy scenario X for cross-section i (m^3/s); $R_{PD}(X)$ is the average PD across all cross-sections for strategy scenario X (%); N is the total number of cross-sections.

(3) Reduction rate of flooding rate (FR)

FR represents the percentage decrease in the proportion of inundated cross-sections when comparing the baseline scenario to the strategy

Table 3

Model calibration and validation results and their validation metrics.

Date	Pingwang station		Zhaotun station		Shangta station	
	Observed	Calculated	Observed	Calculated	Observed	Calculated
2020/6/1	3.02	3.02	2.67	2.67	2.65	2.65
2020/6/2	3.02	2.72	2.67	2.32	2.63	2.29
2020/6/3	3.04	2.72	2.72	2.42	2.64	2.30
2020/6/4	3.06	2.75	2.73	2.43	2.68	2.37
2020/6/5	3.18	2.83	2.96	2.96	2.76	2.50
2020/6/6	3.24	2.98	2.88	2.68	2.90	2.68
2020/6/7	3.23	3.04	2.86	2.65	2.90	2.72
2020/6/8	3.22	3.04	2.89	2.71	2.88	2.74
2020/6/9	3.19	3.04	2.89	2.75	2.87	2.78
2020/6/10	3.16	3.02	2.80	2.75	2.85	2.80
2020/6/11	3.15	3.00	2.79	2.72	2.82	2.82
2020/6/12	3.14	2.99	2.77	2.68	2.79	2.82
2020/6/13	3.09	2.95	2.77	2.67	2.77	2.79
Difference of maximum water levels (m)	0.20		0.00		0.08	
RMSE (m)	0.22		0.19		0.20	

Date	Pingwang station		Zhaotun station		Shangta station	
	Observed	Calculated	Observed	Calculated	Observed	Calculated
2020/9/12	3.28	3.28	2.85	2.85	2.87	2.87
2020/9/13	3.26	3.09	2.85	2.70	2.85	2.65
2020/9/14	3.25	3.11	2.86	2.71	2.84	2.67
2020/9/15	3.31	3.16	2.96	3.06	2.90	2.75
2020/9/16	3.39	3.28	3.04	3.11	2.97	2.89
2020/9/17	3.60	3.46	3.18	3.36	3.12	3.11
2020/9/18	3.81	3.65	3.31	3.36	3.31	3.34
2020/9/19	3.74	3.64	3.20	3.23	3.32	3.34
2020/9/20	3.61	3.52	3.09	3.15	3.24	3.26
2020/9/21	3.59	3.39	3.01	3.06	3.15	3.16
2020/9/22	3.58	3.33	2.97	2.92	3.09	3.09
2020/9/23	3.56	3.30	2.96	2.91	3.06	3.09
2020/9/24	3.50	3.29	2.91	2.85	3.02	3.04
Difference of maximum water levels (m)	0.16		0.05		0.02	
RMSE (m)	0.17		0.09		0.09	

Note: The bold data represent the maximum water levels of the station during the calibration period.

scenarios. The formula used is:

$$\begin{cases} FR = \frac{N_{flood}}{N} \times 100\% \\ R_{FR}(X) = \left(\frac{FR_B - FR(X)}{FR_B} \right) \times 100\% \end{cases} \quad (6)$$

Where FR is the flooding rate, representing the proportion of inundated cross-sections (%); N_{flood} is the number of inundated cross-sections; N is the total number of cross-sections; $R_{FR}(X)$ is the FR for strategy scenario X (%); FR_B is the flooding rate in baseline scenario (%) ; $FR(X)$ is the flooding rate in strategy scenario X (%).

3.3.2. Synergistic effect calculation

According to the definition of synergistic effects, they were quantified as the difference between the performance of the combined strategy and the sum of the corresponding individual strategies (Wang et al., 2022). All synergistic effect calculations were based on equivalent intervention extents between combined strategies and their corresponding individual strategies. A positive value indicated the presence of synergistic effect, while a non-positive value indicated no or negative synergistic benefit. Each synergistic effect value was calculated using the following formula:

$$SE(X_{combined}) = R(X_{combined}) - \sum_{i=1}^n R(X_{individual,i}) \quad (7)$$

Where $SE(X_{combined})$ is the synergistic effect value for scenario X using a combined strategy; $R(X_{combined})$ is the performance value for scenario X

using a combined strategy; $R(X_{individual,i})$ is the MWL, PD, or FR performance value for scenario X using the i -th corresponding individual strategies; n is the total number of individual strategies.

4. Results and discussion

4.1. GBGI synergistic effects and their interaction mechanisms

Based on simulation outputs of maximum water levels, peak discharges, and flooding rates across all scenarios (detailed in Appendix B, Table B 0.1), we calculated their performance including MWL, PD, and FR across 20-, 50-, and 100-year return periods (Table 4).

It is notable that gray strategy—whether individually or in combination (green-gray, blue-gray, and green-blue-gray)—provides significant performance contribution. Table 4 shows that the individual gray strategy achieves MWL of 4.77 % (100-year), PD of 2.47 % (100-year), and FR of 16.32 % (20-year). This finding addresses a critical research gap in flood risk management literature, as GBGI synergy under large-scale depoldering has not been systematically analyzed. Our results demonstrate that depoldering is crucial for enhancing climate adaptation in plain river network regions. The effectiveness of depoldering can be attributed to its ability to restore natural flood regulation mechanisms, as previous studies have confirmed that while hydraulic infrastructure within polders reduces flood risk internally, it diminishes the watershed's overall regulation and retention capacity (Gao et al., 2023). This mechanism is further supported by international experience from the Netherlands' *Room for the River* program, which demonstrated similar benefits of strategic infrastructure removal and floodplain

Table 4
Performance and synergistic effect assessment results.

(a) Under 20-year return period						
Scenario	MWL (%)	PD (%)	FR (%)	Synergistic effect for MWL (%)	Synergistic effect for PD (%)	Synergistic effect for FR (%)
Green	0.65	0.20	2.95	–	–	–
Blue	0.33	-0.34	1.44	–	–	–
Gray	2.37	1.16	10.08	–	–	–
Green-blue	0.99	-0.31	4.44	0.01	-0.16	0.04
Green-gray	2.93	1.25	11.48	-0.09	-0.10	-1.55
Blue-gray	4.09	1.08	14.68	1.38	0.27	3.15
Green-blue-gray	4.66	1.11	16.32	1.30	0.10	1.84
(b) Under 50-year return period						
Scenario	MWL (%)	PD (%)	FR (%)	Synergistic effect for MWL (%)	Synergistic effect for PD (%)	Synergistic effect for FR (%)
Green	0.60	0.39	1.65	–	–	–
Blue	0.07	-0.04	0.32	–	–	–
Gray	2.34	1.39	5.75	–	–	–
Green-blue	0.72	0.43	2.04	0.04	0.08	0.06
Green-gray	2.96	1.60	7.97	0.02	-0.18	0.56
Blue-gray	3.94	1.99	10.71	1.53	0.64	4.64
Green-blue-gray	4.56	2.27	13.43	1.54	0.53	5.71
(c) Under 100-year return period						
Scenario	MWL (%)	PD (%)	FR (%)	Synergistic effect for MWL (%)	Synergistic effect for PD (%)	Synergistic effect for FR (%)
Green	0.76	0.05	1.19	–	–	–
Blue	0.11	-0.14	0.15	–	–	–
Gray	2.46	1.37	4.70	–	–	–
Green-blue	0.92	0.08	1.42	0.05	0.18	0.08
Green-gray	3.08	1.58	6.16	-0.14	0.17	0.26
Blue-gray	4.15	2.32	8.46	1.59	1.09	3.61
Green-blue-gray	4.77	2.47	9.76	1.45	1.20	3.72

restoration, providing empirical validation of the effectiveness of depoldering in different hydrological contexts (Bogdan et al., 2022).

The GBGI synergistic effects were further calculated by comparing the performance of combined strategies against the sum of their individual components. As illustrated in Table 4, blue-gray and green-blue-gray strategies consistently demonstrate positive synergistic effects, while green-blue and green-gray combinations often exhibit limited or even negative effects. This observation preliminarily confirms the presence and varying nature of GBGI synergistic effects at the watershed scale.

Specifically, the green-blue-gray strategy generally demonstrates the strongest synergistic effects across all indicators, with MWL increasing by 1.30–1.54 %, PD rising from 0.10 % at the 20-year return period to 1.20 % at the 100-year return period, and FR peaking at 5.71 % at the

50-year return period (Table 4). These gains arise from a three-stage chain reaction unique to polder systems (Fig. 7). First, green infrastructure (woodland) enhances infiltration, reducing initial runoff by 3.4–4.1 % across different return periods. Next, blue infrastructure—internal ditches, ponds, and lakes—captures the remaining runoff, expanding storage capacity from $4.1 \times 10^6 \text{ m}^3$ to $6.9 \times 10^6 \text{ m}^3$ (Appendix C; Table C.1). Finally, the gray strategy (depoldering) removes dikes, sluices, and pumps, transforming closed polders into interconnected units of the watershed network and allowing stored water to contribute dynamically to flood regulation. This tightly coupled sequence—where infiltration, retention expansion and hydrological reconnection reinforce one another—creates a foundation for GBGI interactions.

The blue-gray strategy also exhibits strong synergistic

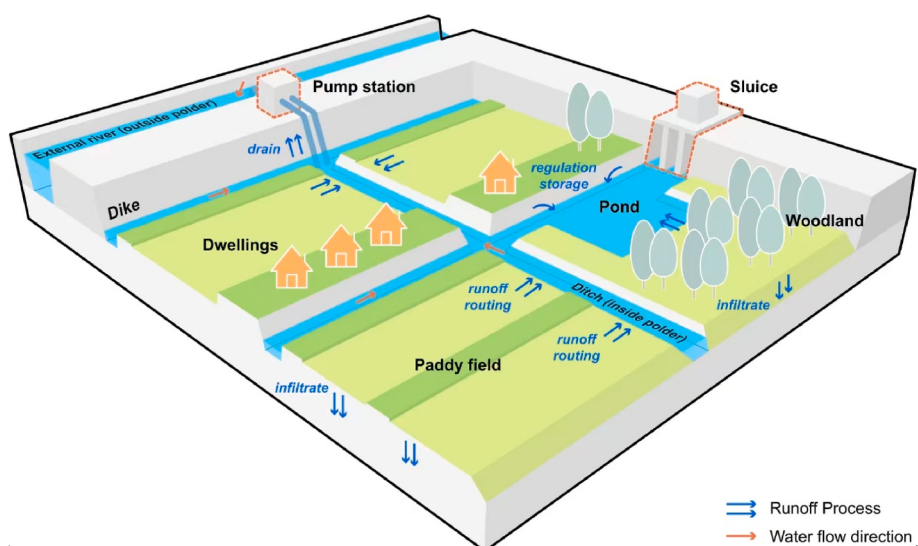


Fig. 7. Runoff processes through the GBGI system in a polder catchment of the Yangtze River Delta.

effects—maximum MWL 1.59 %, PD 1.09 %, FR 4.64 %—contrasting with Wang et al. (2022), who found no blue-gray synergy in micro-scale urban settings. This discrepancy likely stems from distinct interaction mechanisms in the two GBGI systems. In Wang et al.'s study, runoff flows sequentially through gray infrastructure (pipes) to blue infrastructure (storage ponds) without interaction between the two. By contrast, in our polder catchments, gray strategy restores $4.1 \times 10^6 \text{ m}^3$ of storage to the river network, while blue infrastructure expansion simultaneously adds $2.8 \times 10^6 \text{ m}^3$, forming a integrated retention unit rather than a sequential pipe-to-pond flow.

In contrast, the green-gray strategy yields negative synergy, with MWLs of -0.09% at the 20-year and -0.14% at the 100-year return periods, and an FR of -1.55% at the 20-year return period. When only the green strategy is applied, runoff generation drops by $3.4\text{--}4.1\%$, and the polder's $4.1 \times 10^6 \text{ m}^3$ storage volume retains this reduced flow before subsequent discharge. Depoldering removes that storage, causing even the diminished runoff to discharge immediately and thereby offsetting the infiltration benefit.

The green-blue combination shows limited synergistic effects across all indicators. This combination produces minimal synergies for MWL ($0.01\text{--}0.05\%$), variable effects for PD (ranging from -0.16% at the 20-year to 0.18% at the 100-year return period), and negligible effects for FR ($0.04\text{--}0.08\%$) (Table 4). The green strategy reduces runoff generation by $3.7\text{--}4.1\%$, and blue strategy increases storage capacity for the remaining runoff by 68.2% (Appendix C; Table C.1). Because these interventions operate sequentially under unchanged polder hydraulics, their joint effect approximates the sum of individual impacts—resulting in a MWL synergy of only 0.24% .

In summary, these contrasting interaction mechanisms trigger different chain reactions in runoff generation, water retention, and drainage processes, thereby determining the magnitude of synergistic effects for each GBGI combination. For effective climate adaptation and

flood resilience planning, the significant positive synergies observed in blue-gray and green-blue-gray combinations suggest that these approaches should be prioritized in planning frameworks, particularly in areas with similar hydrological characteristics to our study region.

4.2. Spatial heterogeneity of synergistic effects

To investigate the spatial characteristics of these synergistic effects for flood risk management and respond to the planning policy of "reducing external river peak water levels," we visualized the spatial distribution of MWL synergistic effects under the 50-year return period (consistent with the flood protection standard for most of the study area), providing spatial guidance for flood resilience planning. The spatial analysis is based on 13,238 cross-sections across all river channels in the study area, with each cross-section displaying a synergistic effect value. The watershed is characterized by a general west-to-east flow direction, which creates distinct hydrological dynamics across different cross-sections of the river network.

As shown in Fig. 8, significant spatial heterogeneity exists in the synergistic effects across different strategy combinations. The blue-gray and green-blue-gray strategies demonstrate the most substantial positive synergistic effects, particularly in the western and central parts of the watershed. Fig. 8c shows the blue-gray strategy exhibits strong synergistic effects ($0.98\text{--}4.89\%$) in the upstream areas (western region), with an average synergistic effect of 1.53% for MWL (Table 4). Similarly, Fig. 8d illustrates that the green-blue-gray strategy shows prominent positive effects ($1.02\text{--}4.92\%$) with an average synergistic effect of 1.54% for MWL (Table 4).

The stronger synergistic effects observed in upstream areas can be explained by the hydrodynamic characteristics of the watershed. Upstream modifications have a more direct impact on water levels, as there are fewer hydrological influences compared to downstream areas where



Fig. 8. Spatial distribution of MWL synergistic effects under 50-year return period. (a) Green-blue strategy; (b) Green-gray strategy; (c) Blue-gray strategy; (d) Green-blue-gray strategy.

complex water interactions from multiple tributaries occur (Shi et al., 2014). Therefore, the combined blue and gray strategies in upstream areas effectively enhance the conveyance and storage capacity of watershed. Meanwhile, downstream areas experience the cumulative effects of all upstream interventions, potentially creating more complex interactions that may diminish or counteract synergistic effects.

In contrast, the green-blue strategy shows minimal MWL synergistic effects across most cross-sections, with values predominantly below 0.5 % (Fig. 8a) and an average of 0.04 % (Table 4), while Fig. 8b indicates the green-gray strategy displays negative synergies in several eastern river sections (downstream areas) and an average effect of only 0.02 % (Table 4). These variations highlight the importance of location-specific strategy selection.

For practical applications, river sections exhibiting higher synergistic effects should be prioritized for implementation of the corresponding strategy combinations. Importantly, the optimal river sections vary between different strategy combinations, suggesting differentiated spatial planning approaches. Planning targeting on reducing maximum water levels could prioritize blue-gray and green-blue-gray strategies in upstream areas (western region) where these combinations demonstrate the strongest synergistic benefits across the cross-sections.

4.3. Impact of rainfall intensity on synergistic effects

Building on insights from Section 4.1 and 4.2, our analysis reveals how rainfall intensity affects the flood risk management synergistic effects of GBGI strategies across MWLs, PDs, and FRs.

As shown in Fig. 9, the impact of rainfall intensity on flood risk management synergistic effects for different GBGI combinations exhibits unique patterns across the three indicators. The MWL synergies remain largely stable across return periods with values ranging from 1.30 to 1.54 % for green-blue-gray and 1.38–1.59 % for blue-gray strategies (Fig. 9a), indicating minimal sensitivity to changes in rainfall intensity

(only 0.24 % and 0.21 % difference). In contrast, the synergistic effects for PD show greater variability, with an upward trend as return periods increase (Fig. 9b), suggesting that synergies strengthen as rainfall intensifies, with the correlation particularly evident in blue-gray and green-blue-gray strategies, which show increases of 0.82 % and 1.10 % respectively from 20- to 100-year return periods. Additionally, the FR synergies peak at the 50-year return period across all strategies (Fig. 9c). This suggests that strategies targeting FR may perform best at moderate return periods, where GBGI systems reach optimal effectiveness before encountering extreme conditions.

Based on these results, our analysis reveals distinct patterns in the synergistic effects of GBGI strategies across different rainfall intensities, underscoring the need to tailor event-specific GBGI combinations for flood resilience planning—an imperative that grows more urgent as precipitation variability increases under climate change. Under low-intensity events (return period ≤ 20 years), green, blue, and green-blue strategies achieve stable performances, primarily through effective infiltration and storage. This finding suggests that optimizing green and blue infrastructure is effective for managing runoff and minor flooding during frequent events. For moderate events (50-year), the integration of all three infrastructure types reaches peak synergy, with FR synergy reaching 5.71 %. This demonstrates that integrating all three types of infrastructure maximizes flood risk management effectiveness and synergistic effects during moderate rainfall conditions. However, during high-intensity events (100-year), synergistic effect declines significantly, with FRs dropping from 5.71 % (50-year) to 3.72 % (100-year), indicating capacity limitations under extreme conditions. These results suggest that for extreme events, combining blue and gray infrastructure should be prioritized, supported by strategic green infrastructure.

These findings both align with and extend previous research in this field. Cheng et al. (2022) similarly found that under light to moderate rainfall, the green strategy involving Low Impact Development (LID) measures can effectively manage the majority of runoff. Zeng et al.

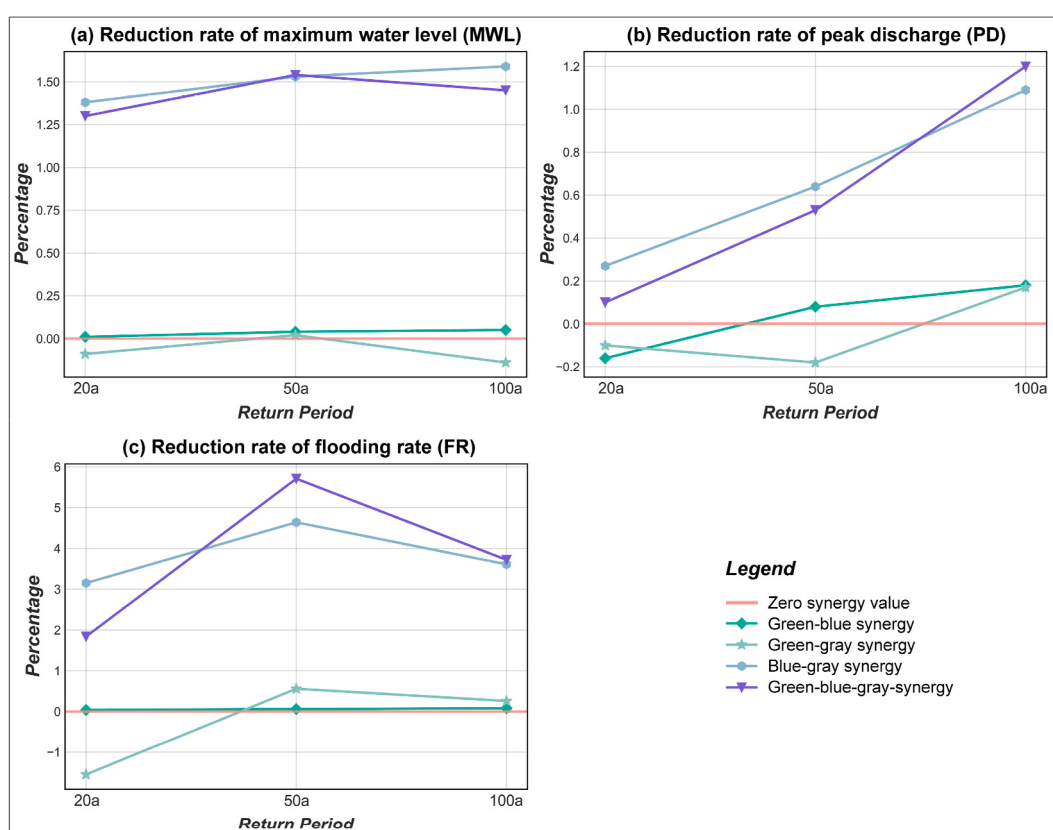


Fig. 9. Synergistic effects of GBGI strategies under different return periods.

(2019) studied the synergistic effects between LID facilities and drainage networks in an urban catchment, finding that LID placement performed better for frequent and low-intensity storms but became less effective during extreme events. Our research advances them by quantifying the synergistic relationships between green, blue, and gray infrastructure across a broader spectrum of rainfall intensities. The differentiation observed across rainfall intensities demonstrates that synergistic mechanisms are not static, but rather dynamic responses to hydrological conditions, significantly advancing theoretical understanding of GBGI systems in watershed-scale contexts.

4.4. Study limitations and expanding the research scope

While this study provides robust evidence for the benefits of combining GBGI strategies, certain limitations must be acknowledged. The primary limitation lies in the data availability and model accuracy. The sparse distribution of hydrological monitoring stations within the study area limits the number of stations available for setting boundary conditions, resulting in suboptimal boundary conditions. This limitation may introduce uncertainties into the model simulations and affect the accuracy of the results. To address these limitations, future research could focus on improving model accuracy through several approaches, such as data interpolation and multi-source data fusion, while integrating satellite-derived data to supplement ground-based measurements under data-scarce conditions.

Another limitation lies in the spatial context and scenario design constraints of this study. The research is confined to the plain river network area of the Yangtze River Delta, where the hydrological and topographical characteristics are unique. The simulations are based on a limited number of specific scenarios and regional conditions, which may not fully capture the complexities of different environments. To address these limitations, future research should extend these findings by simulating a wider range of scenarios as well as diverse environmental contexts. In addition, advanced research methods such as machine learning techniques (H. Chen et al., 2024; Jia and Zhang, 2021) and simulated optimization algorithms (W. Lu et al., 2022) can help identify optimal GBGI combination strategies under various environmental conditions and maximize their flood risk management performance and synergistic effect.

It is also essential to investigate the long-term impacts of GBGI systems, including their maintenance requirements and economic feasibility. Yin et al. (2023) examined how integrated green-blue-gray systems cope with future uncertainties under changing climate conditions, while Bakhshipour et al. (2019) developed a simulation-optimization framework incorporating life cycle costs and sustainability assessments for hybrid drainage systems. In this regard, our current study does not account for lifecycle costs, land use costs, and other economic factors, particularly considering that the large-scale depoldering in our study involves substantial dikes, sluices, and pumps removal, and potential resettlement of communities, which would entail significant socio-economic costs. This limits the applicability of our findings for comprehensive planning and multi-objective decision-making models, which have been developed by other researchers (J. Chen et al., 2024; Martínez et al., 2021; Tansar et al., 2023). Future research should integrate these economic and temporal considerations and incorporate decision-making methods such as TOP-SIS to provide stronger scientific guidance for climate-adaptive infrastructure planning and enhance watershed resilience against evolving flood risks.

5. Conclusions

This study systematically investigates the GBGI synergistic effects for flood risk management in plain river network areas. Our findings reveal several critical insights.

- (1) Gray strategy through large-scale depoldering demonstrates significant flood risk management performance, advancing knowledge on how strategic gray infrastructure removal supports climate adaptation.
- (2) Significant GBGI synergistic effects exist at the watershed scale, but vary across different combinations. Green-blue-gray and blue-gray strategies exhibit positive synergies, while green-blue shows limited synergies and green-gray combinations often demonstrate negative synergistic effects. The underlying mechanisms of these synergistic effects lie in the interactions between infrastructure components within polder systems, particularly in how they influence runoff generation, water retention capacity, and drainage processes.
- (3) Spatial heterogeneity is evident in synergistic effects, with blue-gray and green-blue-gray combinations showing strongest effects concentrated in upstream areas, providing important guidance for location-specific implementation strategies.
- (4) Rainfall intensity affects synergistic effects differently across indicators: MWL shows minimal sensitivity, PD increases with rising intensity, and FR peaks at moderate (50-year) rainfall intensities. These characteristics suggest that green-blue strategies are effective for frequent events, full GBGI integration works best for moderate events, and blue-gray combinations should be prioritized for extreme events.

These findings deepen watershed-scale theory on GBGI synergistic effects and yield location- and event-specific guidance for climate-adaptive infrastructure planning, thereby providing practical pathways to strengthen regional flood resilience through strategically integrated GBGI approaches.

CRediT authorship contribution statement

Haoxun Zhang: Writing – review & editing, Writing – original draft, Software, Methodology, Investigation, Funding acquisition, Formal analysis, Data curation. **Qichen Hong:** Visualization, Software, Methodology, Investigation. **Yutong Jiang:** Software, Methodology, Investigation, Data curation. **Yuting Xie:** Writing – review & editing, Writing – original draft, Supervision, Funding acquisition, Conceptualization.

Declaration of generative AI and AI-assisted technologies in the writing process

During the preparation of this work the authors used ChatGPT and Claude in order to improve readability and language coherence of the manuscript. After using these tools, the authors reviewed and edited the content as needed and take full responsibility for the content of the publication.

Declaration of competing interest

The authors declare that they have no known competing financial interests or personal relationships that could have appeared to influence the work reported in this paper.

Acknowledgements

This work was supported by the Natural Science Foundation of Zhejiang Province [grant number LQ21E080016]; the Scientific Research Fund of Zhejiang Provincial Education Department [grant number Y202352584]; the Center for Balance Architecture, Zhejiang University [grant number KH-20212740]. We sincerely thank the institutions for providing essential data and the referees and editors for their insightful suggestions.

Appendix A. Supplementary data

Supplementary data to this article can be found online at <https://doi.org/10.1016/j.jenvman.2025.126671>.

Data availability

Data will be made available on request.

References

- Al-Humaiqani, M.M., Al-Ghamdi, S.G., 2023. Integrating green-blue-gray infrastructure for sustainable urban flood risk management: enhancing resilience and advantages. In: Al-Ghamdi, S. (Ed.), Sustainable Cities in a Changing Climate, first ed. Wiley, pp. 207–226. <https://doi.org/10.1002/9781394201532.ch13>.
- Alves, A., Gersonius, B., Sanchez, A., Vojinovic, Z., Kapelan, Z., 2018. Multi-criteria approach for selection of green and grey infrastructure to reduce flood risk and increase CO₂-benefits. *Water Resour. Manag.* 32 (7), 2505–2522. <https://doi.org/10.1007/s11269-018-1943-3>.
- Bakhshipour, A.E., Dittmer, U., Haghghi, A., Nowak, W., 2019. Hybrid green-blue-gray decentralized urban drainage systems design, a simulation-optimization framework. *J. Environ. Manag.* 249, 109364. <https://doi.org/10.1016/j.jenvman.2019.109364>.
- Bax, V., van de Lageweg, W.I., Terpstra, T., Buijs, J.M., de Reus, K., de Groot, F., van Schaik, R., Habte, M.A., Schram, J., Hoogenboom, T., 2023. The impact of coastal realignment on the availability of ecosystem services: gains, losses and trade-offs from a local community perspective. *J. Environ. Manag.* 345, 118675. <https://doi.org/10.1016/j.jenvman.2023.118675>.
- Beilicci, E.B.M., Beilicci, R.F., 2024. The study of the variation of the hydrological regime in a representative hydrographic basin during a hydrological cycle. In: 2024 “Air and Water – Components of the Environment” Conference Proceedings, pp. 147–158. https://doi.org/10.24193/AWC2024_14.
- Bijker, W.E., 2002. The oosterschelde storm surge barrier: a test case for Dutch water technology, management, and politics. *Technol. Cult.* 43 (3), 569–584. <https://doi.org/10.1353/tech.2002.0104>.
- Bogdan, E.A., Beckie, M.A., Caine, K.J., 2022. Making room for nature? Applying the Dutch room for the river approach to flood risk management in Alberta, Canada. *Int. J. River Basin Manag.* 20 (2), 153–165. <https://doi.org/10.1080/15715124.2020.1723604>.
- Casal-Campos, A., Sadr, S.M.K., Fu, G., Butler, D., 2018. Reliable, resilient and sustainable urban drainage systems: an analysis of robustness under deep uncertainty. *Environ. Sci. Technol.* 52 (16), 9008–9021. <https://doi.org/10.1021/acs.est.8b01193>.
- Chen, H., Dong, Y., Li, H., Tian, S., Wu, L., Li, J., Lin, C., 2024. Optimized green infrastructure planning at the city scale based on an interpretable machine learning model and multi-objective optimization algorithm: a case study of central Beijing, China. *Lands. Urban Plann.* 252, 105191. <https://doi.org/10.1016/j.landurbplan.2024.105191>.
- Chen, J., Wang, S., Wu, R., 2024. Optimization of the integrated green-gray-blue system to deal with urban flood under multi-objective decision-making. *Water Sci. Technol.* 89 (2), 434–453. <https://doi.org/10.2166/wst.2023.411>.
- Cheng, T., Huang, B., Yang, Z., Qiu, J., Zhao, B., Xu, Z., 2022. On the effects of flood reduction for green and grey sponge city measures and their synergistic relationship—Case study in jinan sponge city pilot area. *Urban Clim.* 42, 101058. <https://doi.org/10.1016/j.uclim.2021.101058>.
- Cheng, W., Wang, C., Zhu, Y., 2006. *Taihu Basin Model*. Hohai University Press in Chinese.
- Cheng, X., Wu, H., 2019. *Flood Risk Scenario Analysis: Methods and Practices*. China Water & Power Press in Chinese.
- China Institute of Water Resources and Hydropower Research, 2010. Guidelines for flood risk mapping compilation. <https://kns.cnki.net/kcms2/article/abstract?v=amOBmv6QLtozAcQ1t-FKFEcGLLkQ452fwip3uNXqjaopxS01P0992d2lRt1tswNcUFURJipjk2FkU16WYz4FtPUKgsqFNsYVs9Jgvq11B6rOf41utN2nbC7b05hK3v9EglgRM-YM0gDxqAhx5lhYU4maT9no92uY8SUZOXh2QbLyIt-ffJCpUxEQ4frI>.
- Disco, C., 2002. Remaking ‘nature’: the ecological turn in Dutch water management. *Sci. Technol. Hum. Val.* 27 (2), 206–235. <https://doi.org/10.1177/016224390202700202>.
- Dong, X., Guo, H., Zeng, S., 2017. Enhancing future resilience in urban drainage system: green versus grey infrastructure. *Water Res.* 124, 280–289. <https://doi.org/10.1016/j.watres.2017.07.038>.
- Drobot, R., Draghia, A., 2014. Coupled hydrological and hydraulic modeling for flood mapping [conference abstract]. EGU general Assembly 2014, Vienna, Austria. *Geophys. Res. Abstr.* 16. <https://doi.org/10.5194/egusphere-egu2014-8055>.
- European Environment Agency, 2023. A transboundary depoldered area for flood protection and nature: Hedwige and prosper polders. Climate-ADAPT. <https://climate-adapt.eea.europa.eu/en/metadata/case-studies/a-transboundary-depoldered-area-for-flood-protection-and-nature-hedwige-and-prosper-polders>.
- Gan, Y., Li, L., Yang, M., 2010. Application of SCS model in runoff calculation in ungauged areas. *Yellow River* 32 (5), 30–31 in Chinese.
- Gao, B., Xu, Y., Sun, Y., Wang, Q., Wang, Y., Li, Z., 2023. The impacts of impervious surface expansion and the operation of polders on flooding under rapid urbanization processes. *Theor. Appl. Climatol.* 151 (3), 1215–1225. <https://doi.org/10.1007/s00704-022-04318-8>.
- Gao, Y., Wu, M., Liu, Y., Gao, L., Zhang, Z., 2023. Analyzing the impact of polder-type flood control pattern on river system’s regulation and storage capacity under urbanization. *JAWRA Journal of the American Water Resources Association* 59 (6), 1219–1245. <https://doi.org/10.1111/1752-1688.13128>.
- Geary, N., 2013. Understanding synergy. *Am. J. Physiol. Endocrinol. Metab.* 304 (3), E237–E253. <https://doi.org/10.1152/ajpendo.00308.2012>.
- Ghofrani, Z., Sposito, V., Faggian, R., 2017. A comprehensive review of blue-green infrastructure concepts. *Int. J. Environ. Sustain.* 6, 15–36. <https://doi.org/10.24102/ijes.v6i1.728>.
- Han, C., Mei, Q., Liu, S., Zhong, G., 2014. Research and application of hydrodynamic coupling model for plain tidal river network. *Journal of Hydrodynamics Series A* 29 (6), 706–712 in Chinese.
- Hosseiniadehatalaei, P., Tabari, H., Willems, P., 2020. Climate change impact on short-duration extreme precipitation and intensity-duration-frequency curves over Europe. *J. Hydrol.* 590, 125249. <https://doi.org/10.1016/j.jhydrol.2020.125249>.
- Hu, Y., Lin, H., Liu, M., 2016. Revision of design storm in Taihu Lake Basin. *J. Hydrol.* 36 (5), 50–53 in Chinese.
- Jia, J., Zhang, X., 2021. A human-scale investigation into economic benefits of urban green and blue infrastructure based on big data and machine learning: a case study of Wuhan. *J. Clean. Prod.* 316, 128321. <https://doi.org/10.1016/j.jclepro.2021.128321>.
- Lan, L., 2023. Study on flood resilient water network planning in Lixiahe Region. *China Rural Water and Hydropower* 2, 108–113+127 in Chinese.
- Li, G., Xiang, X., Tong, Y., Wang, H., 2013. Impact assessment of urbanization on flood risk in the Yangtze River Delta. *Stoch. Environ. Res. Risk Assess.* 27 (7), 1683–1693. <https://doi.org/10.1007/s00477-013-0706-1>.
- Liu, L., 2007. *Study on the Impact of Land Use Change on Runoff and its Water Environment Effects in Shanghai Central Urban Area* [master’s Thesis]. East China Normal University (in Chinese). CNKI.
- Lu, P., Sun, Y., Steffen, N., 2023. Scenario-based performance assessment of green-grey-blue infrastructure for flood-resilient spatial solution: a case study of Pazhou, Guangzhou, greater Bay area. *Lands. Urban Plann.* 238, 104804. <https://doi.org/10.1016/j.landurbplan.2023.104804>.
- Lu, W., Xia, W., Shoemaker, C.A., 2022. Surrogate global optimization for identifying cost-effective green infrastructure for urban flood control with a computationally expensive inundation model. *Water Resour. Res.* 58 (4), e2021WR030928. <https://doi.org/10.1029/2021WR030928>.
- Luo, W., Wang, X., Qiao, W., Sun, J., Qian, L., Fu, H., 2018. Impact of land use change on drainage parameters in plain lake areas based on hydrological-hydrodynamic coupled model. *J. Yangtze River Sci. Res. Inst.* 35 (1), 76–81. <https://doi.org/10.11988/ckyyb.20161226> in Chinese.
- Martínez, C., Vojinovic, Z., Sanchez, A., 2021. Multi-Objective model-based assessment of green-grey infrastructures for urban flood mitigation. *Hydrology* 8 (3). <https://doi.org/10.3390/hydrology8030110>, Article 3.
- Min, VenW., 1985. *Omgaan Met Water. Den Haag: Min VenW.*
- Ncube, S., Arthur, S., 2021. Influence of blue-green and grey infrastructure combinations on natural and human-derived capital in urban drainage planning. *Sustainability* 13 (5), 2571. <https://doi.org/10.3390/su13052571>.
- Pamungkas, A., Purwitaningsih, S., 2019. Green and grey infrastructures approaches in flood reduction. *International Journal of Disaster Resilience in the Built Environment* 10 (5), 343–362. <https://doi.org/10.1108/IJDRBE-03-2019-0010>.
- Rehak, D., Markuci, J., Hromada, M., Barcova, K., 2016. Quantitative evaluation of the synergistic effects of failures in a critical infrastructure system. *International Journal of Critical Infrastructure Protection* 14, 3–17. <https://doi.org/10.1016/j.ijcip.2016.06.002>.
- Rijke, J., van Herk, S., Zevenbergen, C., Ashley, R., 2012. Room for the River: delivering integrated river basin management in the Netherlands. *Int. J. River Basin Manag.* 10 (4), 369–382. <https://doi.org/10.1080/15715124.2012.739173>.
- Rosa, D.W.B., Nascimento, N.O., Moura, P.M., Macedo, G.D., 2020. Assessment of the hydrological response of an urban watershed to rainfall-runoff events in different land use scenarios – Belo Horizonte, MG, Brazil. *Water Sci. Technol.* 81 (4), 679–693. <https://doi.org/10.2166/wst.2020.148>.
- Saeijs, H.L.F., 2008. *Turning the Tide. Essays on Dutch Ways with Water*. Delft Academic Press, Delft.
- Schut, M., Leeuwis, C., van Paassen, A., 2010. Room for the River: room for Research? The case of depoldering De Noordwaard, the Netherlands. *Sci. Publ. Pol.* 37 (8), 611–627. <https://doi.org/10.3152/030234210X12767691861173>.
- Shi, X., Yang, Z., Yan, D., Li, Y., Yuan, Z., 2014. On hydrological response to land-use/cover change in Luanhe River basin. *Adv. Water Sci.* 25 (1), 21–27 in Chinese.
- Soulis, K.X., 2021. Soil conservation service curve number (SCS-CN) method: current applications, remaining challenges, and future perspectives. *Water* 13 (2). <https://doi.org/10.3390/w13020192>, Article 2.
- Suriya, S., Mudgal, B.V., 2012. Impact of urbanization on flooding: the Thirusoolam sub watershed – a case study. *J. Hydrol.* 412–413, 210–219. <https://doi.org/10.1016/j.jhydrol.2011.05.008>.
- Tansar, H., Duan, H.-F., Mark, O., 2023. A multi-objective decision-making framework for implementing green-grey infrastructures to enhance urban drainage system resilience. *J. Hydrol.* 620, 129381. <https://doi.org/10.1016/j.jhydrol.2023.129381>.
- Tavakol-Davani, H., Burian, S.J., Devkota, J., Apul, D., 2016. Performance and cost-based comparison of green and gray infrastructure to control combined sewer overflows. *Journal of Sustainable Water in the Built Environment* 2 (2), 04015009. <https://doi.org/10.1061/JSWBAY.0000805>.
- Van Hemert, M., 2008. *Making Rivers Modular*. University of Twente, Enschede.

- van Staveren, M.F., Warner, J.F., van Tatenhove, J.P.M., Wester, P., 2014. Let's bring in the floods: de-poldering in the Netherlands as a strategy for long-term delta survival? *Water Int.* 39 (5), 686–700. <https://doi.org/10.1080/02508060.2014.957510>.
- Versini, P.-A., Kotelnikova, N., Pouilles, A., Tchiguirinskaia, I., Schertzer, D., Leurent, F., 2018. A distributed modelling approach to assess the use of Blue and Green Infrastructures to fulfil stormwater management requirements. *Landsc. Urban Plann.* 173, 60–63. <https://doi.org/10.1016/j.landurbplan.2018.02.001>.
- Wang, J., Liu, J., Mei, C., Wang, H., Lu, J., 2022. A multi-objective optimization model for synergistic effect analysis of integrated green-gray-blue drainage system in urban inundation control. *J. Hydrol.* 609, 127725. <https://doi.org/10.1016/j.jhydrol.2022.127725>.
- Wang, Y., Xu, Y., Zhang, Q., Li, G., Lei, C., Yang, L., Han, L., Deng, X., 2016. Impact of river network structure changes on storage capacity in Taihu Plain Area. *Acta Geogr. Sin.* 71 (3), 449–458 in Chinese.
- Wiering, M.A., Arts, B.J.M., 2006. Discursive shifts in Dutch river management: 'deep' institutional change or adaptation strategy? *Hydrobiologia* 565, 327–338. <https://doi.org/10.1007/s10750-005-5923-2>.
- Wu, J., Wu, Z., Lin, H., Ji, H., Liu, M., 2020. Hydrological response to climate change and human activities: a case study of Taihu Basin, China. *Water Sci. Eng.* 13 (2), 83–94. <https://doi.org/10.1016/j.wse.2020.06.006>.
- Xu, T., Liu, K., Shan, Y., He, S., 2019. Analysis and countermeasures of flood control situation in river network area of Hangjiahu Plain. *China Rural Water and Hydropower* 2, 123–125 in Chinese.
- Yin, D., Zhang, X., Cheng, Y., Jia, H., Jia, Q., Yang, Y., 2023. Can flood resilience of green-grey-blue system cope with future uncertainty? *Water Res.* 242, 120315. <https://doi.org/10.1016/j.watres.2023.120315>.
- Zeng, S., Guo, H., Dong, X., 2019. Understanding the synergistic effect between LID facility and drainage network: with a comprehensive perspective. *J. Environ. Manag.* 246, 849–859. <https://doi.org/10.1016/j.jenvman.2019.06.028>.
- Zhang, C., Wang, J., Liu, J., Lv, Y., Chen, J., Yang, Z., Zhang, N., 2023. Performance assessment for the integrated green-gray-blue infrastructure under extreme rainfall scenarios. *Frontiers in Ecology and Evolution* 11. <https://doi.org/10.3389/fevo.2023.1242492>. Article 1242492.
- Zhang, M., Peng, D., Lin, H., Qiu, L., 2014. Study on the impact of land use change on runoff in Taihu Lake Basin. *J. Beijing Normal Univ. (Nat. Sci.)* 50 (5), 467–471 in Chinese.
- Zhao, H., Zhou, L., Zhao, R., Li, Z., Qi, Z., 2022. Simulation of flood process in plain area based on MIKE coupling model. *China Rural Water and Hydropower* 7, 97–102 in Chinese.
- Zhong, G., Liu, S., Hu, Z., Zhang, X., 2017. Analysis of the impact of polder drainage on regional flood control in Yangcheng-Dianshan Lake area. *Yangtze River* 48 (21), 9–14. <https://doi.org/10.16232/j.cnki.1001-4179.2017.21.002> in Chinese.